

MULTILEVEL DESCRIPTIVE EXPERIMENT DESIGN REGULARIZATION FRAMEWORK FOR SPARSITY PRESERVING ENHANCEMENT OF RADAR IMAGERY IN HARSH SENSING ENVIRONMENTS

Y.V. Shkvarko, J.I. Yáñez, G.D. Martín del Campo, and V.E. Espadas

Department of Electrical Engineering

Center for Advanced Research and Education of the National Polytechnic Institute, CINVESTAV-IPN

Guadalajara, México

email: shkvarko@gdl.cinvestav.mx

ABSTRACT

We address a new approach to a reconstructive imaging inverse problems solution as required for enhancement of low resolution real aperture radar/fractional SAR imagery in harsh sensing environments. To preserve the image and image gradient map sparsity peculiar for real-world remote sensing (RS) scenarios, we aggregate the minimum risk inspired descriptive experiment design regularization (DEDR) framework for balanced image resolution enhancement over noise suppression with two additional regularization levels: (i) the variational analysis inspired minimization of the image total variation (TV) map and (ii) the sparsity preserving regularizing projections onto convex solution sets (POCS). The new framework incorporates the TV metric structured regularization into the weighted ℓ_2 metric structured DEDR data agreement objective function and suggests the solver for the overall reconstructive imaging inverse problem employing the DEDR-TV-POCS-restructured MVDR strategy. The DEDR-TV-POCS method implemented in an implicit iterative fashion outperforms the competing nonparametric adaptive radar imaging techniques both in the resolution enhancement and computational complexity reduction as verified in the reported simulations.

Index Terms—Descriptive experiment design regularization, fractional synthetic aperture radar (F-SAR), image enhancement, remote sensing, total variation.

1. INTRODUCTION

1.1. Motivation

Conventional low resolution real aperture radar (RAR) and unfocused fractional synthetic aperture radar (F-SAR) systems with simple and cheap hardware are attractive in many low cost remote sensing (RS) missions with small airborne and/or unmanned aerial vehicle platforms [1–5]. In modern RS computational imaging applications [6–15], the enhancement of low resolution RS imagery is stated and treated in a framework of nonparametric inverse problems

of reconstructing the backscattered wavefield spatial spectrum pattern (SSP) i.e., the scene average power reflectivity (the second order statistics of the random reflectivity of the 2-D remotely sensed scene) referred to as its radar image [3–5]. In harsh sensing environments, the SSP recovery inverse problem solution is complicated due to the random perturbations in the signal formation operator (SFO) that cause multiplicative degradations with the statistics usually unknown to the observer [4,7,9].

1.2. New challenges in relation to prior work

The challenge of this study is to develop a new approach for solving the inverse problem of feature enhanced SSP recovery from the low resolution RAR/F-SAR imagery acquired in a harsh sensing environment taking different path from the previous studies [11–22]. The idea is to incorporate into the existing frameworks [16,17,20] additional feature enhancing, i.e., sparsity preserving (Sp-Pr) and convergence guaranteed regularization modalities. Our approach is based on the descriptive experiment design regularization (DEDR) framework [16,17] for the balanced RS image resolution enhancement over noise suppression. Next, to preserve image and image gradient map sparsity peculiar for typical real-world remotely sensed scenes, we incorporate into such DEDR approach two additional regularization modalities: (i) the variational analysis (VA) inspired minimization of the recovered image total variation (TV) map and (ii) the Sp-Pr and convergence guaranteed regularizing projections onto convex solution sets (POCS) [6,8,20]. Thus, the first innovative proposition of this paper consists in an extension of the recently proposed dynamic DEDR approach [20] for the scenarios with the piecewise smooth sparse SSP distributions. The second innovative proposition relates to the construction of the aggregated multilevel regularization framework with the user controlled degrees of freedom that balances the attained spatial resolution over composite noise suppression and guarantees the image sparsity preservation. At the heart of this approach is the proposal to restructure the metric in the solution set via inducing the aggregated weighted ℓ_2 –TV

metric for the RS image and the image gradient maps. Algorithmically, this task is performed via incorporating into the DEDR-restructured robust minimum variance distortionless response (MVDR) framework [10] the additional ℓ_2 -TV and POCS regularization levels different from the previously proposed ℓ_2 and ℓ_1 structured DEDR-related approaches [10–17,19–22]. We corroborate that the new aggregated DEDR-TV-POCS-restructured robust MVDR method implemented in the constructed implicit contractive mapping iterative computing mode outperforms the competing nonparametric adaptive feature-enhanced radar imaging techniques in the literature, e.g., the robust MVDR [12,17], the ℓ_2 only structured APES [19,20], the ℓ_1 only structured DEDR [21] and the dynamic DEDR [20,21] that do not aggregate the POCS with the ℓ_2 -TV structured regularization, as we demonstrate in the reported numerical simulations of enhancement of a speckle corrupted low resolution F-SAR image.

2. SSP RECONSTRUCTION PROBLEM

2.1. Observation data model

Following [9,11,16], consider the vector-form coherent equation of observation that relates the lexicographically ordered random scene reflectivity \mathbf{e} observed through the $M \times K$ perturbed matrix-form SFO $\tilde{\mathbf{S}} = \mathbf{S} + \Delta_{\mathbf{S}}$ and degraded by noise \mathbf{n} with the RAR/SAR trajectory data signal

$$\mathbf{z} = \tilde{\mathbf{S}}\mathbf{e} + \mathbf{n} = \mathbf{S}\mathbf{e} + \Delta_{\mathbf{S}}\mathbf{e} + \mathbf{n}. \quad (1)$$

The regular SFO term \mathbf{S} is specified by the employed modulation format [4,8,9], and $\Delta_{\mathbf{S}}$ represents the zero mean random SFO perturbation term. In (1), \mathbf{e} , \mathbf{n} , \mathbf{z} are random zero-mean vectors composed of the decomposition coefficients $\{e_k\}_{k=1}^K$, $\{n_m\}_{m=1}^M$ and $\{z_m\}_{m=1}^M$, respectively [8] characterized by the correlation matrices, $\mathbf{R}_{\mathbf{e}} = \mathbf{D}(\mathbf{b}) = \text{diag}(\mathbf{b})$, $\mathbf{R}_{\mathbf{n}} = N_0 \mathbf{I}$, and $\mathbf{R}_{\mathbf{z}} = \langle \tilde{\mathbf{S}}\mathbf{R}_{\mathbf{e}}\tilde{\mathbf{S}}^+ \rangle + \mathbf{R}_{\mathbf{n}}$, correspondingly, where $\langle \cdot \rangle$ defines the averaging over the randomness of the SFO, superscript $+$ stands for Hermitian conjugate, and N_0 is the power of the white observation noise vector \mathbf{n} . Vector \mathbf{b} composed of the elements, $\{b_k = \langle |e_k|^2 \rangle\}_{k=1}^K$, is a lexicographically ordered vector-form representation of the SSP over the pixel framed 2-D x - y scene $\{k_x = 1, \dots, K_x; k_y = 1, \dots, K_y; k = 1, \dots, K = K_x K_y\}$ with the correspondingly ordered SFO matrix in (1). In the considered standard (not compressed) RAR/F-SAR data acquisition scenarios [1–5], $M \geq K$.

2.2. Inverse problem phenomenology

The nonlinear inverse problem for recovery of the SSP vector \mathbf{b} from the available data recordings \mathbf{z} , i.e.,

$\hat{\mathbf{b}} = \text{est}_{\text{strategy}}\{\mathbf{b} | \mathbf{z}\}$, depends on the employed estimation *strategy*. In the basic DEDR framework [16], the SSP estimation $\hat{\mathbf{b}} = \text{est}_{\text{DEDR}}\{\mathbf{b} | \mathbf{z}\}$ is performed in the positive convex cone solution set $\mathbb{B}_{(K)}$ in the Euclidian space with the metric structure induced by the ℓ_2 scalar product

$$\|\mathbf{b}\|_{\ell_2} = [\mathbf{b}, \mathbf{b}]^{1/2} = \left(\sum_{k_x=1, k_y=1}^{K_x, K_y} (b(k_x, k_y))^2 \right)^{1/2} \quad (2)$$

which does not involve the image TV norm. The feature-enhanced SSP recovery implies the development of a framework (in this study, the unified DEDR-TV-POCS-restructured robust MVDR method) and the related technique(s) for high-resolution estimation (feature-enhanced reconstruction) of the SSP

$$\hat{\mathbf{b}} = \text{est}_{\text{DEDR-TV-POCS}}\{\mathbf{b} | \mathbf{z}\} \quad (3)$$

from the available recordings (1) of the complex (coherent) trajectory data \mathbf{z} degraded by the composite noise (multiplicative $\Delta_{\mathbf{S}}$ and additive \mathbf{n}) with the SFO perturbation statistics $\langle \tilde{\mathbf{S}}\mathbf{D}(\mathbf{b})\tilde{\mathbf{S}}^+ \rangle$ usually unknown to the observer [4,9]. To perform the feature enhanced recovery (3) we suggest the VA inspired re-definition of the metric structure in the image/solution set $\mathbb{B}_{(K)} \ni \mathbf{b}, \hat{\mathbf{b}}$ that features the piecewise SSP gradient map smoothness properties peculiar to the majority of the real-world RS scenes [1,4,9,18,20]. Thus, we construct the VA-inspired metric structure in the image/solution set via inducing the following weighted balanced ℓ_2 -type and TV-type norms

$$\|\mathbf{b}\|_{\mathbb{B}_{(K)}} = m_{\ell_2} ([\mathbf{b}, \mathbf{b}] + [\mathbf{b}, \nabla^2 \mathbf{b}])^{1/2} + m_{\text{TV}} \|\mathbf{b}\|_{\text{TV}}. \quad (4)$$

Here, the term with the weight factor m_{ℓ_2} specifies the equibalanced image \mathbf{b} and image gradient $\nabla \mathbf{b}$ ℓ_2 -type norm specified via the (Hermitian positive definite) discrete Laplacian operator ∇^2 [8]. The term with the weight factor m_{TV} induces the image TV norm component computed via the finite differences (D_x, D_y over the x and y image axes $\|\mathbf{b}\|_{\text{TV}} = \sum_{k_x, k_y} (|D_x b(k_x, k_y)|^2 + |D_y b(k_x, k_y)|^2)^{1/2} = \|\nabla \mathbf{b}\|_{\ell_1}$ treated as an ℓ_1 norm of vector \mathbf{b}_{gr-m} formed of the magnitudes of the image gradient vector entries returned by operator $|\nabla \bullet|$, i.e., $\mathbf{b}_{gr-m} = |\nabla \mathbf{b}|$ [6]. In (4), factors m_{ℓ_2} and m_{TV} control the balance between two metrics measures. The conventional ℓ_2 only structured metric (2) relates to (4) as its simplest version for the assignments $m_{\ell_2} = 1$, $m_{\text{TV}} = 0$ and excluded gradient ℓ_2 norm term in (4).

3. UNIFIED DEDR-TV-POCS FRAMEWORK

3.1. DEDR restructured MVDR

The high-resolution adaptive estimation of the SSP via the classical adaptive minimum variance distortionless response (MVDR) method [10,19] employs the strategy

$$\hat{b}_k = \frac{1}{\mathbf{s}_k^+ \mathbf{R}_z^{-1}(\mathbf{b}) \mathbf{s}_k} ; k = 1, \dots, K \quad (5)$$

optimal (in the MVDR sense) for the theoretical model-dependent (\mathbf{b} -dependent) covariance matrix inverse $\mathbf{R}_z^{-1}(\mathbf{b})$

where \mathbf{s}_k^+ defines the so-called k th steering vector composed of the corresponding k th row ($k = 1, \dots, K$) of the adjoint regular SFO matrix \mathbf{S}^+ [10,16]. In the real-world RS imaging scenarios, the unknown exact model of the covariance matrix $\mathbf{R}_z(\mathbf{b})$ is substituted by its sample maximum likelihood (ML) estimate [5] $\mathbf{Y} = \hat{\mathbf{R}}_z = (1/J) \sum_{j=1}^J \mathbf{z}_{(j)} \mathbf{z}_{(j)}^+$ that yields the conventional MVDR algorithm [10,19]

$$\hat{b}_k = \frac{1}{\mathbf{s}_k^+ \mathbf{Y}^{-1} \mathbf{s}_k} ; k = 1, \dots, K \quad (6)$$

feasible for the full rank \mathbf{Y} only. From simple algebra, it is easy to corroborate that the theoretical model based strategy (5) is algorithmically equivalent to the solution (with respect to the SSP vector \mathbf{b}) of the nonlinear equation

$$\{\mathbf{D}(\mathbf{b})\}_{\text{diag}} = \{\mathbf{W}(\mathbf{b}) \mathbf{R}_z(\mathbf{b}) \mathbf{W}(\mathbf{b})\}_{\text{diag}} \quad (7)$$

with the solution operator (SO)

$$\mathbf{W}(\mathbf{b}) = (\mathbf{D}(\mathbf{b}) \mathbf{S}^+ \mathbf{S} + N_0 \mathbf{I})^{-1} \mathbf{D}(\mathbf{b}) \mathbf{S}^+ . \quad (8)$$

Substituting in (7) the theoretical covariance matrix \mathbf{R}_z by its ML sample estimate $\mathbf{Y} = \hat{\mathbf{R}}_z$ yields the DEDR-restructured MVDR strategy

$$\begin{aligned} \hat{\mathbf{b}} \rightarrow \text{solution to the Eq.} \rightarrow \{\mathbf{D}(\hat{\mathbf{b}})\}_{\text{diag}} &= \{\mathbf{W}(\hat{\mathbf{b}}) \mathbf{Y} \mathbf{W}(\hat{\mathbf{b}})\}_{\text{diag}} \\ &= \{\mathbf{K}(\hat{\mathbf{b}}) \mathbf{Q} \mathbf{K}(\hat{\mathbf{b}})\}_{\text{diag}} \end{aligned} \quad (9)$$

with the solution independent sufficient statistics matrix $\mathbf{Q} = \mathbf{S}^+ \mathbf{Y} \mathbf{S}$ and the solution dependent self adjoint matrix-form reconstructive operator

$$\mathbf{K} = \mathbf{K}(\hat{\mathbf{b}}) = (\mathbf{D}(\hat{\mathbf{b}}) \mathbf{\Psi} + N_0 \mathbf{I})^{-1} \mathbf{D}(\hat{\mathbf{b}}) . \quad (10)$$

In (7), (9), operator $\{\cdot\}_{\text{diag}}$ returns the vector of the principal

diagonal of the embraced matrix, and in (10), $\mathbf{\Psi} = \mathbf{S}^+ \mathbf{S}$ represents the matrix-form point spread function (PSF) of the low-resolution matched spatial filtering (MSF) image formation system [1,5,8]. Note that matrix \mathbf{K} does not involve inversion of $\mathbf{D}(\hat{\mathbf{b}})$, hence, the DEDR-restructured MVDR strategy (9) results in the desired Sp-Pr technique that admits zero entries in \mathbf{b} and is feasible for rank deficient data matrices \mathbf{Y} (for $J < M$).

The DEDR framework [16,17] suggests the worst case statistical performances optimization approach to the problem (3) with the model uncertainties regarding the statistics of the SFO perturbations that yields the robust SO

$$\mathbf{W}(\hat{\mathbf{b}}) = \mathbf{K}(\hat{\mathbf{b}}) \mathbf{S}^+ = (\mathbf{D}(\hat{\mathbf{b}}) \mathbf{\Psi} + N_\Sigma \mathbf{I})^{-1} \mathbf{D}(\hat{\mathbf{b}}) \mathbf{S}^+ , \quad (11)$$

in which $N_\Sigma = N_0 + \beta$ is the observation noise power N_0 augmented by factor $\beta \geq 0$ adjusted to the regular SFO Loewner ordering factor and the statistical uncertainty bound for the SFO perturbation (see [16] for details). Hence, the robust modification of the DEDR is constructed by replacing in (9), (10) N_0 by the composite (loaded) $N_\Sigma = N_0 + \beta$. In practical estimation scenarios, this regularization factor N_Σ can be evaluated empirically from the speckle corrupted low-resolution MSF image following one of the local statistics techniques exemplified in [17].

Next, we adapt the robust DEDR-restructured MVDR (9) to the single look mode ($J = 1$) substituting \mathbf{Y} by the rank-1 $\mathbf{z} \mathbf{z}^+$ and defining the complex MSF imaging system output

$$\mathbf{q} = \mathbf{S}^+ \mathbf{z} , \quad (12)$$

in which case the solver (9) is transformed into

$$\hat{\mathbf{b}} \rightarrow \text{solution to the Eq.} \rightarrow \hat{\mathbf{b}} = \{\mathbf{K}(\hat{\mathbf{b}}) \mathbf{q} \mathbf{q}^+ \mathbf{K}(\hat{\mathbf{b}})\}_{\text{diag}} . \quad (13)$$

From simple algebra, it can be next shown that for $\mathbf{b} = \{\mathbf{D}(\mathbf{b})\}_{\text{diag}}$, self adjoint \mathbf{K} (10) and rank-1 $\mathbf{Y} = \mathbf{z} \mathbf{z}^+$, the solver (13) is algorithmically equivalent to the following robust modified DEDR-restructured MVDR solver

$$\hat{\mathbf{b}} \rightarrow \text{solution to the Eq.} \rightarrow \mathbf{\Phi}(\hat{\mathbf{b}}) \hat{\mathbf{b}} = \mathbf{A}(\hat{\mathbf{b}}) \mathbf{g} = \mathbf{f}(\hat{\mathbf{b}}) , \quad (14)$$

in which

$$\mathbf{g} = \{\mathbf{q} \mathbf{q}^+\}_{\text{diag}} , \quad (15)$$

$$\mathbf{A} = \mathbf{A}(\hat{\mathbf{b}}) = \mathbf{D}^2(\hat{\mathbf{b}}) , \quad (16)$$

$$\mathbf{f} = \mathbf{f}(\hat{\mathbf{b}}) = \mathbf{A}(\hat{\mathbf{b}}) \mathbf{g} , \quad (17)$$

$$\mathbf{\Phi} = \mathbf{\Phi}(\hat{\mathbf{b}}) = (\mathbf{D}(\hat{\mathbf{b}}) \mathbf{\Psi} + N_\Sigma \mathbf{I}) \bullet (\mathbf{D}(\hat{\mathbf{b}}) \mathbf{\Psi} + N_\Sigma \mathbf{I})^* \quad (18)$$

where symbol \bullet defines the Schur-Hadamard (element wise) matrix product.

Remark. The standard MVDR solver (6), hence its DEDR-restructured versions (13), (14) seek for the solutions in the positive cone set with the ℓ_2 metric structure defined by (2). Thus, all those are unable to perform feature enhanced SSP recovery in the ℓ_2 -TV restructured solution set $\mathbb{B}_{(K)}$ (4).

3.2. Aggregated DEDR-TV-POCS technique

To construct the feature enhanced unified DEDR-TV-POCS solver (3) in the solution set $\mathbb{B}_{(K)}$ with the aggregated metric structure (4) we incorporate into (14) the composite cascade transform $\mathcal{T} = \mathcal{P}_{+\pi} \mathcal{M} \mathcal{P}_{DF}$. The action of such \mathcal{T} is threefold. First, the local statistics-based despeckling filter [17] \mathcal{P}_{DF} transforms the speckle corrupted MSF image (15) into the despeckled low resolution image $\hat{\mathbf{b}}_{[0]} = \mathcal{P}_{DF} \mathbf{g}$ that serves as an input (zero-step iteration) for the further iterative reconstructive processing. Second, \mathcal{M} transforms (14) into the implicit contractive mapping iterative scheme with three corresponding discrepancy terms related to the ℓ_2 -TV structured (4). Last, $\mathcal{P}_{+\pi}$ is a hard thresholding operator that at each iteration $i = 1, \dots$ clips off all entries of $\hat{\mathbf{b}}_{[i]}$ lower than the user specified nonnegative Sp-Pr tolerance threshold level π . Hence, $\mathcal{P}_{+\pi}$ serves as a convergence guaranteed POCS operator [8,20]. With such cascade \mathcal{T} the (14) is transformed into the implicit iterative feature enhanced DEDR-TV-POCS technique

$$\begin{aligned} \hat{\mathbf{b}}_{[i+1]} = & \hat{\mathbf{b}}_{[i]} + \mathcal{P}_{+\pi} \{c_1(\mathbf{f}_{[i]} - \Phi_{[i]} \hat{\mathbf{b}}_{[i]}) + c_2 \nabla^2[\mathbf{f}_{[i]} - (\Phi_{[i]} \hat{\mathbf{b}}_{[i]})] \\ & + c_3[|\nabla \mathbf{f}_{[i]}| - |\nabla(\Phi_{[i]} \hat{\mathbf{b}}_{[i]})|]\}; \quad i = 1, \dots, I \end{aligned} \quad (19)$$

different from other competing approaches [16–21]. Instead of two weights m_{ℓ_2} , m_{TV} in (4), here we have incorporated three regularization factors c_1 , c_2 , c_3 that balance the discrepancy terms in (19). The iterative process is initialized with $\hat{\mathbf{b}}_{[0]} = \mathcal{P}_{DF} \mathbf{g}$ and is terminated at $\hat{\mathbf{b}}_{[I]}$ for which the user specified ℓ_2 -norm convergence tolerance level ε_{TL} is attained at some $i = I$. In the simulations, we specified $\varepsilon_{TL} = 0.03$ and treated different feasible assignments to c_1 , c_2 , c_3 .

4. SIMULATIONS AND DISCUSSIONS

Fig. 1 reports simulations results of enhancement of an F-SAR image applying different DEDR-related techniques. The test 1024×1024-pixel high resolution image of Fig. 1(a) borrowed from the real-world SAR imagery [23] relates to the hypothetical full focused SAR imaging mode. The low resolution speckle corrupted image of the same scene presented in Fig. 1(b) corresponds to the single look F-SAR mode (quick look modality (15)) for the typical operational

scenario specifications, similar to the comparative previous studies [17,20] as specified in the Figure captions. Figs. 1(c) thru 1(f) report the feature-enhanced radar imaging results obtained with different compared DEDR-related techniques specified in the Figure captions. These results verify that the best perceptual F-SAR image enhancement performances as well as quantitative signal-to-noise improvement ($SNI = 10 \log_{10}(\|\mathbf{q} - \mathbf{b}\|_{\ell_2}^2 \cdot \|\hat{\mathbf{b}} - \mathbf{b}\|_{\ell_2}^{-2})$) measures and convergence rates (compared to the related competing studies) are attained with the developed DEDR-TV-POCS technique.

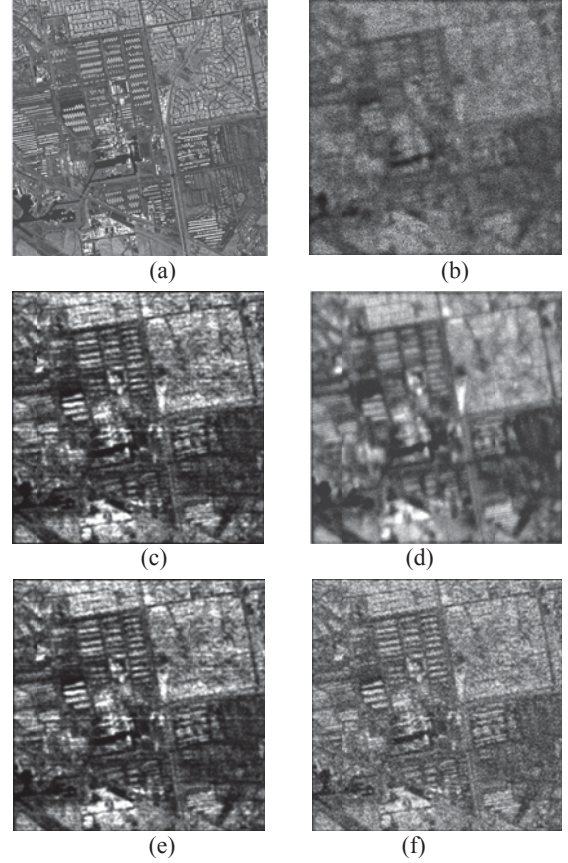


Fig. 1. Simulation results: (a) high resolution test scene borrowed from [23]; (b) low resolution speckle corrupted MSF image of the same scene formed with the simulated F-SAR; modeled system parameters: triangular range PSF (the width at $\frac{1}{2}$ of the peak value, $\kappa_y = 20$ pixels); Gaussian bell azimuth PSF (the width at $\frac{1}{2}$ of the peak value, $\kappa_x = 40$ pixels); single-look scenario with the fully developed speckle, SNR = 0 dB; (c) image enhanced applying the ℓ_2 only DEDR-restructured APES method [19] ($c_1 = 1$, $c_2 = c_3 = 0$; convergence at $I = 22$, $SNI = 8.44$ dB); (d) image enhanced with the TV-inspired ℓ_1 only structured DEDR method [21] ($c_1 = c_2 = 0$, $c_3 = 1$; convergence at $I = 28$, $SNI = 5.23$ dB); (e) image enhanced using the most competing ℓ_2 only structured dynamic DEDR-VA technique [20] ($c_1 = c_2 = 1$, $c_3 = 0$; convergence at $I = 16$, $SNI = 10.8$ dB); (f) image enhanced with the DEDR-TV-POCS technique (19) applying the zero-level threshold operator \mathcal{P}_{0} (equibalanced case with $c_1 = c_2 = c_3 = 1$; convergence at $I = 8$, $SNI = 14.06$ dB).

5. REFERENCES

- [1] L.G. Cutrona, *Synthetic Aperture Radar*, in *Radar Handbook*, 2nd ed., M.I. Skolnik, Ed. in chief, MA: McGraw Hill, 1990.
- [2] A. Farina, *Antenna-Based Signal Processing Techniques for Radar Systems*, Norwood, MA: Artech House, 1991.
- [3] D.R. Wehner, *High-Resolution Radar*, 2nd ed., Boston, MA: Artech House, 1994.
- [4] A. Ishimaru, *Wave Propagation and Scattering in Random Media*. NY: IEEE Press, 1997.
- [5] F.M. Henderson and A. V. Lewis, Eds., *Principles and Applications of Imaging Radar, Manual of Remote Sensing*, NY: Wiley, 3d ed., vol. 3, 1998.
- [6] J.H. Mathews, *Numerical Methods for Mathematics, Science, and Engineering, Second Edition*, Englewood Cliffs, NJ: Prentice Hall, 1992.
- [7] S.W. Perry, H.S. Wong, and L. Guan, *Adaptive Image Processing*, NY: CRS Press, 2001.
- [8] H.H. Barrett.; K.J. Myers, *Foundations of Image Science*, NY: Willey, 2004.
- [9] G. Franceschetti and R. Landari, *Synthetic Aperture Radar Processing*. NY: Wiley, 2005.
- [10] A.B. Gershman, "Robustness issues in adaptive beamforming and high-resolution direction finding," in *High-Resolution and Robust Signal Processing*, Yihgo Hua, A.B. Gershman, and Qi Chen Eds., NY- Basel: Marcel Dekker, 2004.
- [11] Y.V. Shkvarko, "Unifying regularization and Bayesian estimation methods for enhanced imaging with remotely sensed data—Part I: Theory", *IEEE Trans. Geoscience and Remote Sensing*, vol. 42, No. 5, pp. 923-931, 2004.
- [12] Y.V. Shkvarko, "Unifying regularization and Bayesian estimation methods for enhanced imaging with remotely sensed data— Part II: Implementation and performance issues", *IEEE Trans. Geoscience and Remote Sensing*, vol. 42, No. 5, pp. 932-940, 2004.
- [13] P. Perona and J. Malik, "Scale-space and edge detection using anisotropic diffusion", *IEEE Trans. Pattern Anal. Machine Intell.*, vol. 12, No. 7, pp. 629-639, 1990.
- [14] M.J. Black, G. Shapiro, D.H. Marimont, and D. Heeger, "Robust anisotropic diffusion", *IEEE Trans. Image Proc.*, vol. 7, No. 3, pp. 421-432, 1998.
- [15] S. John and M.A. Vorontsov, "Multiframe selective information fusion from robust error theory", *IEEE Trans. Image Proc.*, Vol. 14, No. 5, pp. 577-584, 2005.
- [16] Y.V. Shkvarko, "Unifying experiment design and convex regularization techniques for enhanced imaging with uncertain remote sensing data—Part I: Theory", *IEEE Trans. Geoscience and Remote Sensing*, vol. 48, No. 1, pp. 82-95, 2010.
- [17] Y.V. Shkvarko, "Unifying experiment design and convex regularization techniques for enhanced imaging with uncertain remote sensing data —Part II: Adaptive implementation and performance issues", *IEEE Trans. Geoscience and Remote Sensing*, vol. 48, No. 1, pp. 96-111, 2010.
- [18] V.M. Patel, G.R. Easley, D.M. Healy, and R. Chellappa, "Compressed synthetic aperture radar", *IEEE Journal of Selected Topics in Signal Proc.*, vol. 4, No. 2, pp. 244-254, 2010.
- [19] T. Yarbidi, J.; Li, P. Stoica.; M. Xue and A.B. Baggeroer, "Source localization and sensing: A nonparametric iterative adaptive approach based on weighted least squares", *IEEE Trans. Aerospace and Electronic Syst.*, vol. 46, No. 1, pp. 425-443, 2010.
- [20] Y.V. Shkvarko, J. Tuxpan, and S.R. Santos, "Dynamic experiment design regularization approach to adaptive imaging with array radar/SAR sensor systems", *Sensors*, vol. 2011, No 5, pp 4483-4511, 2011.
- [21] Y.V. Shkvarko, J. Tuxpan, and S.R. Santos, "High-resolution imaging with uncertain radar measurement data: A doubly regularized compressive sensing experiment design approach", in *Proc. IEEE 2012 IGARS Symposium*, ISBN: 978-1-467311-51/12, pp. 6976-6970, Munich, Germany, July 2012.
- [22] V. Ponomaryov, A. Rosales, F. Gallegos, and I. Loboda, "Adaptive vector directional filters to process multichannel images", *IEICE Trans. Communications*, vol. E90-B, No. 2, pp. 429-430, Feb. 2007.
- [23] *TERRAX-SAR Images*, Available at: <http://www.astrium-geo.com/en/19-gallery?img=1690&search=gallery&type=0&sensor=26&resolution=0&continent=0&application=0&theme=0>.